

Proceedings of the Tenth Asian Congress of Fluid Mechanics
17–21, May 2004, Peradeniya, Srilanka.

FLUX SCALING AND PLUME STRUCTURE IN HIGH Ra - HIGH Sc TURBULENT CONVECTION

Baburaj A. Puthenveetil and Jaywant H Arakeri

Department of Mechanical Engineering, Indian Institute of Science,
Bangalore, India 560012

ABSTRACT: The arrangement of brine above water across a micro porous permeable membrane is used to study high Rayleigh Number ($10^{11} - 10^{10}$) high Schmidt number (650) turbulent convection. The flux shows $4/3^{rd}$ scaling with line plume as the near wall coherent structures. Shifting of multiple large scale flow cells result in changing near membrane mean shear directions for large aspect ratios. Lower aspect ratios show single large scale flow cell and constant sense of mean shear.

1. INTRODUCTION

In Rayleigh - Benard convection, where buoyancy is the only source of motion, the non dimensional heat flux, Nusselts number (Nu) can be expressed as a function of the independent non dimensional parameters viz. Rayleigh number (Ra) which expresses the ratio of buoyancy forces to the dissipative effects, Prandtl number (Pr), a fluid property and Aspect Ratio (AR = Length/Height), a geometric parameter. When Rayleigh number is high, turbulent convection occurs with a well-mixed core and surface boundary layers. The classical $4/3^{rd}$ law which states that flux $\sim \Delta T^{4/3}$ (ie. $Nu \sim Ra^{1/3}$) is obtained from the assumption that transport process is determined only by the near wall boundary layers and hence is independent of layer height h. At the same time, as very high Ra implies negligible dissipative effects, dimensional consistency demands $Nu \sim (RaPr)^{1/2}$. The experimentally observed scaling law is $Nu = K Ra^n$ where n is slightly less than $1/3$, resulting in a weak dependence of flux on layer height. At $Ra > 10^8$ the system is seen to generate a large-scale mean flow which modifies the near wall diffusive boundary layers by shear effects, and is expected to be the reason for the observed value of n. Plumes play the major role in transporting heat in this regime from the boundary layer.¹³ Various phenomenological explanations, each involving major assumptions, viz. a plume dominated mixing zone,² a turbulent shear boundary layer,¹⁰ a Blasius laminar boundary layer with dominant balance of bulk and boundary layer dissipation⁶ etc seem to be able to obtain the observed scaling.

The Prandtl number dependence of Nu at high Pr is not clear. The only studies are that of Goldstein⁵ using naphthalene mass transfer technique at Schmidt number of 2750 and of Askenazi and Steinberg¹ at Pr of 93. The $Ra^{1/3}$ scaling was observed by Goldstein till $Ra < 10^{13}$, while Askenazi's studies seem to support an exponent less than $1/3$. At very high Pr, as the viscous boundary layers reach their limiting thickness, it is expected that Nu becomes independent of Pr.⁷ In this case the flux is expected to follow the $4/3$ law as the strength of large scale flow reduces with increasing Prandtl Number. Hence, in addition to the large number of unresolved issues about the nature of high Rayleigh number turbulent free convection, few studies exist for the high Prandtl

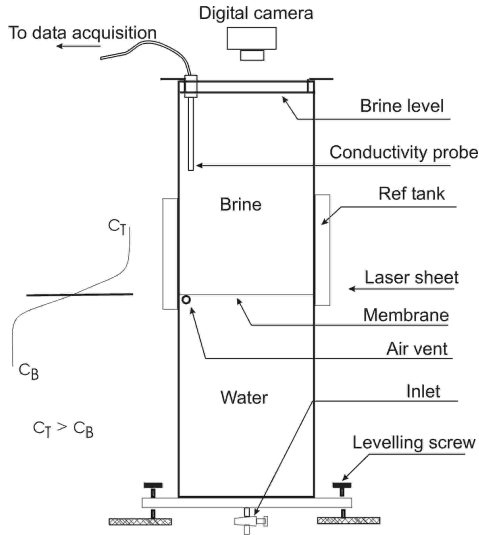


Figure 1: Experimental setup

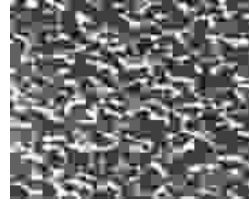


Figure 2: SEM image of Pall GelmanTM membrane

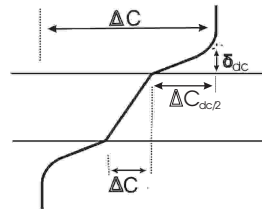


Figure 3: Diffusion drop across the membrane

Number regime. Further, very little is known about the nature of near wall coherent structures in this regime.

We study high Ra turbulent free convection driven by density difference across a thin permeable horizontal partition separating two tanks of square plan form cross sections. The gravitational potential due to a heavier fluid (brine) above a lighter fluid (water) across the partition drives the flow, which is resisted by the presence of the micro porous partition. At low pore sizes in the membrane, the transport across the partition would become diffusion dominated, while the transport above and below the partition becomes similar to turbulent convection above flat horizontal surfaces. As molecular diffusivity (D) of NaCl is about 100 times lower than temperature diffusivity, larger values of Ra and Sc are achieved through this arrangement for similar driving density potentials. The structure of convection in this case can easily be visualised. In this paper we report the flux scaling and the nature of near wall coherent structures in high Rayleigh number ($\sim 10^9$ to 10^{13}) high Schmidt number (~ 650) turbulent convection.

2. EXPERIMENTAL SETUP AND MEASUREMENTS

A schematic representation of the experimental setup is shown in Figure 1. The test section, made of 8mm float glass, has two vertical compartments, with ground mating edges and a permeable partition fixed in between them. Figure 2 shows a ($1000\times$) scanning electrode microscope (SEM) image of Pall GelmanTMNX29325 membrane disc filters used in the experiments. These are bilayer membranes made of nylon66 with 0.45μ mean pore size and thickness of 142.24μ . The solidity of the membrane was calculated as 0.6 from the SEM images by computing the occupied fraction of pixels of a binary image generated from figure 2, based on a suitably chosen threshold.

The top tank is filled with brine after the bottom tank is filled distilled water. To reduce initial mixing, a temporary tank with sponge bottom is kept over the membrane while the top tank is filled, the removal of which initiates the experiment. A thin transparent plexiglass sheet floating over the brine level prevents evaporation and produces similar boundary conditions for the two compartments. The side glass compartments hold distilled water to reduce excessive refraction of the laser beam during visualisation. The assembly is mounted on a levelling table so that the

partition can be made horizontal. Test section cross sections of 15 cms× 15cms, and 10cms × 10cms with height 23 cms, ie aspect ratios of 0.652 and 0.435 were used.

The flux is estimated from the transient measurement of the the top tank concentration. Assuming that the fluid in both the compartments is well mixed in the region away from the partition, and using the mass balance at any time $C_T(t) V_T + C_B(t) V_B = C_T^0 V_T + C_B^0 V_B$, with $C_B^0 = 0$, the concentration difference is

$$\Delta C(t) = C_T(t) - C_B(t) = (1 + \frac{V_T}{V_B})C_T(t) - C_T^0 \frac{V_T}{V_B} \quad (1)$$

Here, V_T is the top tank solution volume, V_B the bottom tank solution volume, $C_T(t)$ is the top tank concentration, $C_B(t)$ is the bottom tank concentration and the superscript ⁰ denotes initial values. The nett flux of NaCl across the partition at any instant is given by the rate of change of top tank concentration as

$$q = -h \frac{dC_T}{dt} \quad (2)$$

where h is the top compartment height. Hence, ΔC and flux can be calculated from the transient measurement of concentration of top tank fluid.

The concentration of NaCl in the top tank is estimated from the measurement of electrolytic conductivity of the top tank fluid. The conductivity measurements are made by ORION SENSOR-LINK TMPCM100 conductivity measurement system,⁹ with a 2 electrode conductivity cell, model ORION TM011050, with automatic temperature compensation. The probe was calibrated before each experiment. As calculation of $\frac{dc}{dt}$ directly from the measured C_T vs t distribution results in excessive errors due to data noise an exponential decay fit is used calculate the derivative $\frac{dC_T}{dt}$.

The plume structure was visualised by Laser Induced fluorescence of Sodium Fluorescein dye. The bottom tank solution was tagged with the dye and a horizontal laser sheet(Spectra-Physics, Stabilite 2017TMAr-Ion,5W) was passed just above the partition. The dye in the bottom solution, while convecting upwards, fluoresces on incidence of the laser beam to make the plume structure visible. The quantity of dye (1.2ppm) was chosen to give sufficient fluorescence intensity without affecting the measured conductivity. The fluorescence images were captured on a digital camera (SONY PCR 9E) after cutting off the laser light wave lengths using a yellow glass filter, Coherent optics OG-515.

3. RESULTS AND DISCUSSION

3.1 Flux

To compare the scaling of flux with that of high Rayleigh number turbulent free convection, the driving potential in the present case is corrected for the concentration drop occuring across the partition, as shown in figure 3. This concentration drop is $\Delta c_m = q l_m / (\Gamma D)$ where Γ = open area factor of the membrane, l_m = the thickness of the membrane. Therefore, effective concentration difference on one side of the partition $\Delta c_{dc}/2 = (\Delta c - \Delta c_m)/2$. We look at the scaling of flux with $(\Delta \rho / \rho)_{dc}/2 = \beta \Delta C_{dc}/2$ in the form of an alternate representation of flux. Hereafter, the subscript _{dc} denotes this corrected effective concentration difference.

Figure 4 shows the variation of flux with the effective driving potential obtained in the experiments. The calculations were conducted after correcting the measured concentration curve for systematic shifts due to change in probe linearity. The error bars, which include random and systematic errors, for flux and ΔC shown in the plot indicate the extent of possible variation. The plot includes the results for experiments with a starting concentration of $C_T^0 = 10g/l$ at the two aspect ratios of 0.652 and 0.435, as well as experiments with starting concentration of $C_T^0 = 3g/l$ for AR=0.652. Therefore, within the present accuracy of the measurements, the flux

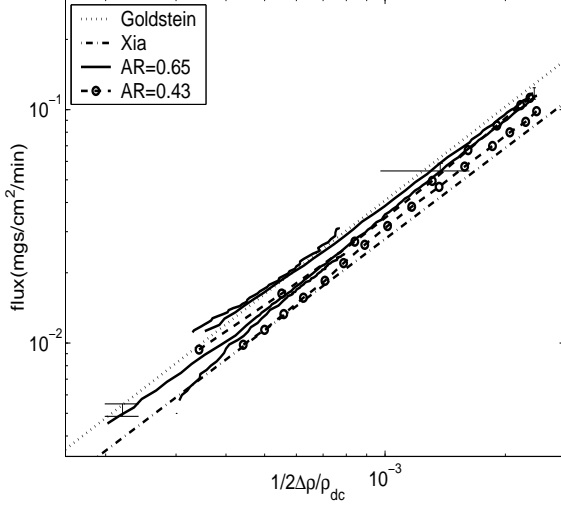


Figure 4: Variation of flux with $\frac{1}{2} \left(\frac{\Delta\rho}{\rho} \right)_{dc}$

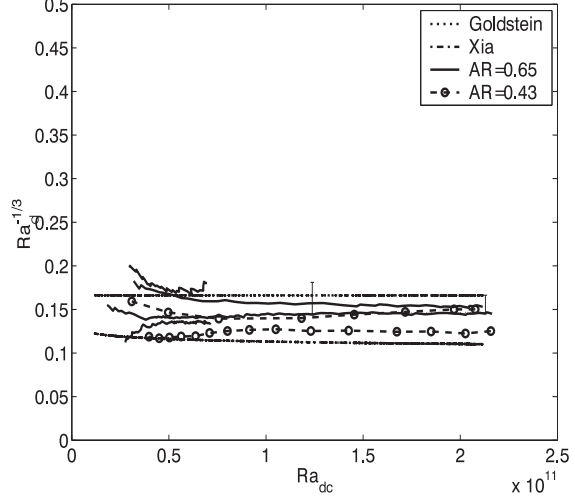


Figure 5: Variation of $Ra_\delta^{-1/3}$ with Ra_{dc}

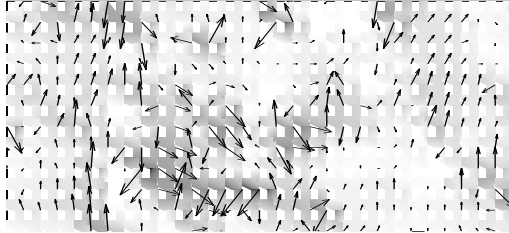
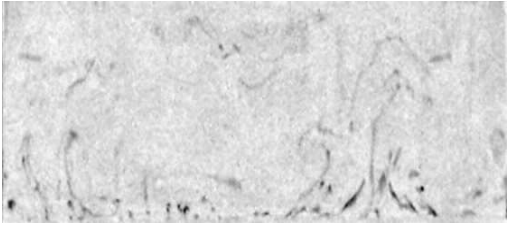
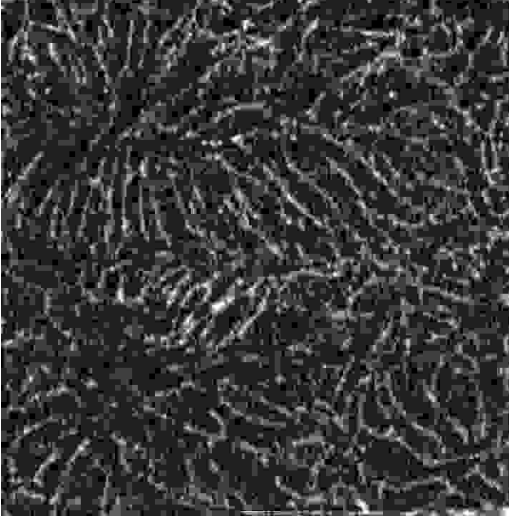
seems to be independent of the starting concentration and the aspect ratio. The figure also shows the corresponding results of Goldstein⁵ and Xia.⁸

Theerthan¹² have shown that a more appropriate representation of non dimensional flux in turbulent free convection is in terms of $Ra_\delta^{-1/3}$, where Ra_δ is the Rayleigh Number based on the diffusion layer thickness, δ_d . The diffusion layer thickness for the current case is calculated as $\delta_{dc} = (D\Delta c_{dc}/2)/q$. $Ra_\delta^{-1/3}$ can be written as a ratio of two fluxes as,

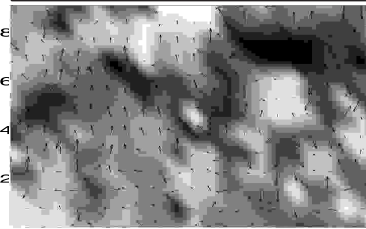
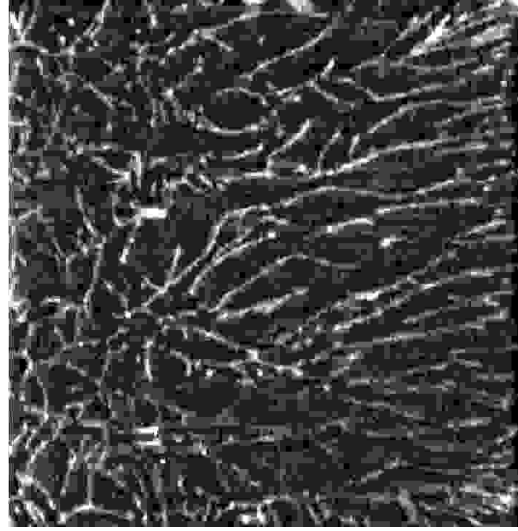
$$Ra_\delta^{-1/3} = q / \left(\frac{D\Delta C_{dc}/2}{Z_w} \right), \quad \text{where, } Z_w = \left(\frac{\nu D}{g\beta\Delta C_{dc}/2} \right)^{1/3} \quad (3)$$

is a near wall length scale for turbulent free convection.¹¹ This representation does not have the layer height as a parameter and hence is a better representation in turbulent free convection where near wall phenomena decides the flux. $Ra_\delta^{-1/3}$ varies only between 0.1 and 0.3 for a wide range of Ra and various types of free convection, being a reflection of the fact that heat flux in turbulent free convection for a given ΔT and fluid does not vary much. It could be noticed from (3) that $Ra_\delta^{-1/3}$ is a constant if flux scales as $\Delta C^{4/3}$.

Figure 5 shows the variation of $Ra_\delta^{-1/3}$ with Rayleigh number using the effective concentration difference, Ra_{dc} for the same experiments as in figure 4. The line $Ra_\delta^{-1/3} = 0.166$ is obtained from the correlation $Nu = 0.066Ra^{1/3}$ of Goldstein⁵ at $Pr=2750$. The relation of Xia, $Nu=0.14Ra^{0.297}Pr^{-0.03}$ is also plotted in the figure. The current experimental values of $Ra_\delta^{-1/3}$ are nearly constant implying that the flux scales as the $4/3^{rd}$ power of ΔC_{dc} . Goldsteins value of $Ra_\delta^{-1/3}$ falls within the error range of the current experiments. The deviation from the constant $Ra_\delta^{-1/3}$ for very low Ra_{dc} seen in figure 5 cannot be inferred to be from the change in the flux scaling, as the errors involved in calculating $\frac{\Delta\rho}{\rho}$ becomes large when the concentration differences between the tanks tend to zero. Therefore, we conclude from the present experiments that Rayleigh Numbers of $10^{11} - 10^{10}$ at Schmidt number of 650, the flux scales very nearly as $\Delta C^{4/3}$, and the effect of Schmidt number on flux is negligible. To get a better understanding of the phenomena, we now study the near wall dynamics of coherent structures in the current experiments.



Velocity cm/s



Velocity(cm/s)

Figure 6: Multiple large scale flow cells at AR=0.65 (a)Horizontal planform of plume structure at $Ra_{dc} = 4.07 \times 10^{11}$, $\frac{\Delta\rho}{\rho_{dc}} = 4.52 \times 10^{-3}$. Image size is 15cms \times 15 cms (b)Vertical plume structure at $Ra_{dc} = 4.06 \times 10^{11}$, $\frac{\Delta\rho}{\rho_{dc}} = 4.5 \times 10^{-3}$ image size is 15cm \times 6.7 cms (c)Velocity distribution for(b)

Figure 7: Single large scale flow cell at AR=0.435 (a)Horizontal planform of plume structure at $Ra_{dc} = 4.068 \times 10^{11}$, $\frac{\Delta\rho}{\rho_{dc}} = 4.515 \times 10^{-3}$ Image size is 10cms \times 10 cms (b)Vertical plume structure at $Ra_{dc} = 4.1003 \times 10^{11}$, $\frac{\Delta\rho}{\rho_{dc}} = 4.551 \times 10^{-3}$ Image size is 7.25cms \times 4.67 cms (c)Velocity distribution for(b)

3.2 Coherent structures

Figure 6(a) shows the plan form plume structure, obtained when the upcoming plumes intersect a horizontal laser sheet very near ($<1\text{mm}$) the membrane. The image shows the full test section cross section of 15cm \times 15cm (AR = 0.65) and is at $Ra_{dc} = 4.0711 \times 10^{11}$ and $\frac{\Delta\rho}{\rho_{dc}} = 4.6 \times 10^{-3}$, where the flux follows $4/3^{\text{rd}}$ law (see figure 5). The figure shows that the near wall coherent structures in high Rayleigh number convection are line plumes. We notice that the plume structure display circular patches of aligned lines originating from a plume free area in the center. The

aligned nature of the plume lines implies the presence of a near wall flow along these lines. The predominant motion of the fluid in these patches, as observed from the video images, were outward from the plume free circular area along the plume lines. The lateral shift of the plumes lines, due to the entrainment velocity of the nearby line plumes, was also very low ($\sim 1\text{mm/s}$). Hence we infer these cells as the signatures of large scale flow cells. The large scale flow impinges on the plume free circular area in the center of each aligned plume region and create an outward near membrane flow which aligns the line plumes. The current image shows two large scale flow cells on the right side of the image. These large scale flow cells shift their position randomly, implying that the large scale flow direction in high Ra convection, at least for higher AR, is not constant.

The above picture would be more clear from Figure 6(b) which shows the plume structure in a vertical plane at 2cms from a side wall of the test section, (ie 2cms from the bottom of figure 6(a)). Note that Figure 6(a) is after 11.5 minutes from figure 6(b), so that the latter figure is not the exact vertical view of the former. The height of figure 6(b) is 6.7 cms. The figure shows that plumes combine giving rise to columns of upward rising fluid, which results in a downward travelling portion of fluid in between the columns, which impinges on the wall and create the near wall shear. Figure 6(c) shows the near wall velocity field vectors (overlaid over the velocity magnitude) estimated using the spatial intensity correlation technique⁴ between figure 6(b) and another image 0.4 seconds later. The upward moving columns and the resulting downward impingement in between them could be noticed from the figure. The column rise velocity is about 0.3 cms/s while the downward velocities are much larger ($\sim 0.8\text{ cms/s}$). It is known that the large scale velocity scales as the Deardorff's velocity scale $W_* = (g\beta qh)^{1/3}$. ³ W_* for Figure 6(c) is 0.31 cms/s, of the same order as the plume rise velocity. Hence, one could infer that the large scale flow velocity is essentially driven by plume columns, which inturn organise the plume structure. The current study shows that the mean shear near the walls could be larger than that due to W_* as the downward velocities between the plume columns are higher than W_* .

The planform plume structure at AR=0.435 is shown in figure 7(a). The image size is the same as the test section cross section of 10cms \times 10 cms. Figure 7(b) shows the vertical plume structure 13 min prior to figure 7(a). The image shows a vertical section (normal to plume structure in figure 7(a)) 2cms above the bottom side of figure 7(a) of 7.25cms width and 4.67 cms height starting from the left of figure 7(a). The plan form plume structure and the vertical image lead us to the inference that there is a single large scale flow cell spanning the full tank cross section. The large scale flow impinges on the membrane on the right and creates a near membrane velocity from right to left. This results in inclined plumes near the membrane as seen in the vertical image. Plumes combine and rise along the left wall, feeding the mean circulation, which sustains the mean shear near the membrane. The velocity estimates in figure 7(c) from spatial correlation between images 0.4 seconds apart reproduces the dynamics reasonably well, with the plume column rise velocity at the LHS of the figure ($\sim 0.3\text{cms/s}$) being of the same order as the large scale flow velocity estimated as the Deardorff scale (0.31cms/s).

4. CONCLUSIONS

Experiments show that the flux scaling in high Rayleigh Number -high Schmidt number turbulent convection, even in the presence of a large scale flow, follows the $4/3^{rd}$ law and seems to have little dependence on Sc. The flux is only weakly dependent on the AR. The near wall coherent structures are line plumes. We detect multiple large scale flow cells and changing large scale flow direction at higher AR. Lower AR shows a single large scale flow cell and constant sense of near membrane mean shear. The large scale flow is shown to be sustained by rising columns of combined plumes, the velocity of which scales as Deardorff scale.

REFERENCES

- [1] Ashkenazi S and Steinberg V: High Rayleigh number turbulent convection in a gas near the gas-liquid critical point *Physical Review Letters* November 1999 **83**(18), 3641–3644
- [2] Castaing.B et.al: Scaling of hard thermal turbulence in Rayleigh-Bernard convection *Jl Fluid Mech* 1989 **204**, 1–30
- [3] Deardorff J W: Convective velocity and temperature scales for the unstable planetary boundary layer and for Rayleigh convection *Journal of the Atmospheric Sciences* November 1970 **27**, 1211–1213
- [4] Gendrich C P and Koochesfahani M M: A spatial correlation technique for estimating velocity fields using molecular tagging velocimetry *Experiments in Fluids* 1996 **22**, 67–77
- [5] Goldstein R J et.al: High Rayleigh-number convection in a horizontal enclosure *Jl Fluid Mech* 1990 **213**, 111–126
- [6] Grossman S and Lohse D: Scaling in thermal convection : A unifying theory *Jl Fluid Mech* 2000 **407**, 27
- [7] Grossmann S and Lohse D: Thermal convection for large Prandtl numbers *Physical Review Letters* April 2001 **86**(15), 3316–3319
- [8] Ke-Qing Xia, Siu Lam and Sheng-Qi Zhong: Heat flux measurement in high Prandtl number turbulent Rayleigh Benard convection *Physical Review Letters* 2002 **88**(6), 064501
- [9] ORION Research Inc.: *SensorlinkTM Model PCM100 Instruction manual*
- [10] Shraiman B I and Siggia E D: Heat transport in high Rayleigh number convection *Physical Review A* September 1990 **42**(6), 3650–3653
- [11] Teerthan S A: *Turbulent free convection over horizontal surfaces* Ph.D. thesis Dept of Mech Engg, IISc, Bangalore November, 1997
- [12] Teerthan S A and Arakeri J H: Plan form structure and heat transfer in turbulent free convection over horizontal surfaces *Phys Fluids* 2000 **Vol 12**, pp 884 –894
- [13] Theerthan S A and Arakeri J H: A model for near wall dynamics in turbulent rayleigh - benard convection *Jl Fluid Mech* 1998 **373**, 221 –254